Published in final edited form as:

Nature. 2014 November 20; 515(7527): 443–447. doi:10.1038/nature13713.

Discovery and characterization of small molecules that target the Ral GTPase

Chao Yan[1], **Degang Liu**[2], **Liwei Li**[2], **Michael F. Wempe**[3], **Sunny Guin**[1], **May Khanna**[2], **Jeremy Meier**[4], **Brenton Hoffman**[4], **Charles Owens**[1], **Christina L. Wysoczynski**[5], **Matthew D. Nitz**[6], **Eric W. Knabe**[2], **David L. Brautigan**[6], **Bryce M. Paschal**[7], **Martin A. Schwartz**[8], **David Jones**[5], **David Ross**[3], **Samy O. Meroueh**[2,9], and **Dan Theodorescu**[1,5,10]

[1]Department of Surgery, University of Colorado, Aurora, CO, 80045

[2]Department of Biochemistry, Indiana University School of Medicine, Indianapolis, IN 46202

[3]Department of Pharmaceutical Sciences, University of Colorado, Aurora, CO, 80045

[4]Cardiovascular Research Center, University of Virginia, Charlottesville VA 22908

[5]Department of Pharmacology, University of Colorado, Aurora, CO, 80045

[6]Department of Microbiology, Immunology, and Cancer Biology, University of Virginia, Charlottesville, VA, 22908

[7]Department of Biochemistry and Molecular Genetics, University of Virginia, Charlottesville, VA, 22908

[8]Departments of Cardiology and Cell Biology, Yale University, New Haven, CT, 06511

[9]Department of Chemistry and Chemical Biology, Indiana University Purdue University Indianapolis, Indianapolis, IN 46202

[10]University of Colorado Comprehensive Cancer Center, Aurora, CO, 80045

Abstract

The Ras-like GTPases RalA and B are important drivers of tumor growth and metastasis[1]. Chemicals that block Ral function would be valuable as research tools and for cancer therapeutics. Here, we used protein structure analysis and virtual screening to identify drug-like molecules that bind a site on the GDP-form of Ral. Compounds RBC6, RBC8 and RBC10 inhibited Ral binding

Correspondence and requests for materials should be addressed to Dan Theodorescu, University of Colorado Comprehensive Cancer Center, Aurora, CO 80045, Phone: (303)724-7135, FAX: (303)724-3162, dan.theodorescu@ucdenver.edu.

AUTHOR CONTRIBUTIONS

D.T. conceived the initial screening idea/concept.
S.O.M. executed the initial screen idea and delivered the 88 “hits”.
D.T., S.O.M., and D.R. coordinated the project.
C.Y., L.L., M. K., E. W. K, D. L., J.M., B.H., M.D.N., B.M.P., D. L. B., S.G., C.O., C.L.W performed experimental work and data analysis.
M.F.W performed and analyzed the pharmacokinetic and pharmacodynamics experiments.
D.J. performed and analyzed the NMR experiments.
C.Y., D.T., S.O.M., D.L.B., B.M.P. and M.A.S. wrote the manuscript.

The authors declare no competing financial interests.

to its effector RalBP1, Ral-mediated cell spreading in murine fibroblasts and anchorage-independent growth of human cancer cell lines. Binding of RBC8 derivative BQU57 to RalB was confirmed by isothermal titration calorimetry, surface plasma resonance and ^{15}N-HSQC NMR. RBC8 and BQU57 show selectivity for Ral relative to Ras or Rho and inhibit xenograft tumor growth similar to depletion of Ral by siRNA. Our results show the utility of structure-based discovery for development of therapeutics for Ral-dependent cancers.

More than one-third of human tumors harbor activating *RAS* mutations[2], which has motivated extensive efforts to develop inhibitors of Ras for cancer therapy. However, therapies directed at interfering with Ras post-translational modifications[3] gave poor clinical performance and efforts shifted to target signaling components downstream of Ras such as Raf-MEK-ERK mitogen-activated protein kinases[4] and the phosphoinositide 3-kinase-AKT-mTOR pathway[5]. A third pathway downstream of Ras that leads to activation of the Ras-like small GTPases, RalA and RalB[6], has not been targeted to date. Active Ral activates cellular processes through effectors including Ral Binding Protein 1 (RalBP1, RLIP76 or RIP1[7]), Sec5/Exo85, filamin, and phospholipase D1[8–10]. These effectors mediate regulation of cell adhesion (anchorage independence), membrane trafficking (exocytosis, endocytosis), mitochondrial fission and transcription. RalA and RalB are important drivers of the proliferation, survival and metastasis of multiple human cancers including skin[11], lung[12], pancreatic[1], colon[13], prostate[14], and bladder[15,16].

We set out to discover small molecules that inhibit the intracellular actions of Ral GTPases. Our approach was based on the hypothesis that molecules that selectively bind to Ral-GDP might restrict Ral in an inactive state in the cell, making it unavailable to promote processes linked to tumorigenesis. Comparing available three-dimensional structures of RalA revealed differences in a region adjacent to, but distinct from, the guanine nucleotide binding pocket (Fig. 1). This site is formed by the switch-II region (Ral^{70}-Ral^{77}), helix α2 (Ral^{78}-Ral^{85}) and one face of helix α3 (Fig. 1a). Its proximity to the previously described C3bot binding site[17] supports the notion that small molecule occupancy at this site could inhibit function. The crystal structures used in the comparison included RalA-GDP (PDB code 2BOV, Fig. 1a, b) and RalA-GNP (non-hydrolysable form of GTP) in complex with exo84 (PDB code 1ZC4, Fig. 1c) or sec5 (PDB code 1UAD, Fig. 1d). Volumes calculated for this binding site were 175 Å^3 for RalA-GDP (Fig. 1b), 155 Å^3 for RalA-GNP-exo84 (Fig. 1c), and 116 Å^3 for RalA-GNP-sec5 (Fig. 1d). To our knowledge, a RalB-GDP crystal structure is not available. However, in the RalB-GNP structure (PDB code 2KE5, Extended Data Fig. 1) this binding site is largely absent. Next, we used a structure-based virtual screening approach[18] to identify small molecules that bind to this site in RalA-GDP by individually docking 500,000 compounds to this site (ChemDiv, v2006.5)[19] and scoring protein-ligand complexes based on calculated interaction energies. This process led to selection of 88 compounds.

We developed an ELISA for assay of Ral activity in living cells based on selective binding of active RalA-GTP to its effector protein RalBP1. This assay used J82 human bladder cancer cells stably expressing FLAG-tagged RalA. The epitope tag greatly increased the sensitivity and dynamic range of the assay compared to using Ral antibodies for detection (Extended Data Fig. 2a). Cells were treated with each of the 88 compounds (tested at 50

μM), extracts prepared, and FLAG-RalA binding to recombinant RalBP1 immobilized in 96 well plates was quantified. In this assay, the RalA binding reflects its GTP-loading and capacity for effector activation. Compounds RBC6, RBC8, and RBC10 (structures shown in Fig. 1e–g) reduced the activation of RalA in living cells (Fig. 1h) while compounds RBC5, RBC7, and RBC42 (structures not shown) had no effect and thus served as negative controls. None of the 88 compounds inhibited GTP or GDP binding to purified recombinant RalA (Supplementary Information), consistent with the interaction site being distinct from that used for binding guanine nucleotides.

A second cell-based assay also assessed the effects of compounds. Ral is required for lipid raft exocytosis and spreading of murine embryonic fibroblasts (MEFs) on fibronectin-coated coverslips[20]. In these cells, depletion of RalA by siRNA inhibits spreading of WT MEFs, whereas caveolin deficient ($Cav1^{-/-}$) MEFs are resistant to RalA depletion. When RBC6, RBC8 and RBC10 were tested for effects on cell spreading in WT and $Cav1^{-/-}$ MEFs, inhibition was observed only in the WT MEFs (Fig. 1i, Extended Data Fig. 2b). RBC6 and RBC8 are related structures sharing the same bicyclic core (Fig. 1e, f), with specific substitutions giving rise to similar but somewhat different binding orientations in the allosteric binding cavity (Extended Data Fig. 2c–e). We therefore focused on the RBC6/8 for further studies.

To test for direct binding of compounds to Ral, we used TROSY (Transverse Relaxation-Optimized Heteronuclear Single Quantum Coherence) ^{15}N-HSQC NMR. The NMR structure of RalB in complex with the GTP analogue GMP-PNP (GNP) has been solved (PDB code 2KE5, BMRB entry 15230)[21], therefore we focused on this isoform. First, we obtained complete backbone NMR chemical shift assignments for the RalB-GDP complex (see methods) and then compared the ^{15}N-HSQC NMR spectrum of RalB-GDP and RalB-GNP to determine chemical shift differences between the Ral GTP vs. GDP bound states. Almost all the differences were confined to residues that interact with the third phosphate of the GTP (Extended Data Fig. 3a, b). ^{1}H-^{15}N-HSQC spectra were then recorded in the presence of the compound RBC8 or DMSO as a control and chemical shift changes compared. RBC8 induced chemical shift changes in RalB-GDP but not RalB-GNP, indicating that RBC8 shows selectivity for the GDP bound form of Ral (Extended Data Fig. 3c, d). Moreover, RBC5, which did not affect the level of active Ral in the cell-based ELISA assay, also did not induce chemical shift changes in RalB-GDP (Extended Data Fig. 3e), therefore serving as additional negative control. Based on all data including structural features, a series of RBC8 derivatives was synthesized and tested for binding *in vitro*. We chose BQU57 for further evaluation because of its superior performance compared to RBC8 and its drug-like properties (Fig. 2a, Extended Data Fig. 4a, synthesis pathway in Supplementary Information). A detailed NMR analysis of the binding between BQU57 and RalB-GDP was carried out. The NMR spectrum of RalB-GDP (100 μM) in the absence (black) and presence (magenta) of 100 μM BQU57 is shown in Fig. 2b. Concentration-dependent chemical shift changes for representative residues are shown in Fig. 2c. A plot of the chemical shift changes with 100 μM BQU57 as a function of sequence (Fig. 2d) shows that residues that exhibit significant changes (highlighted bars) are located in the switch-II (aa 70–77) and helix α2 (aa 78–85) region. Because no RalB-GDP crystal structure is

available, instead a homology model was generated based on the similarity to RalA-GDP, and the residues that displayed chemical shift changes in response to the compounds were mapped onto this model (Fig. 2e). The majority of the chemical shift changes localized to the allosteric site, consistent with assignment of BQU57 binding to this site based on modeling. Similar to results with RBC8, BQU57 (100 μM) did not bind to RalB-GNP (100 μM) as indicated by minimal chemical shift changes on NMR spectrum (Extended Data Fig. 4b). Analysis of the NMR chemical shift titrations revealed that binding of BQU57 was stoichiometric up to the apparent limiting solubility of the drug (estimated as ~100 μM in control experiments without protein)(Extended Data Fig. 4c). The binding of BQU57 to RalB-GDP also was determined using Isothermal Titration Calorimetry (ITC) which yielded a K_D = 7.7 ± 0.6 μM (Fig. 2f). This was similar to results from Surface Plasma Resonance (SPR) which gave a K_D of 4.7 ± 1.5 μM (Extended Data Fig. 4d).

Next we evaluated RBC8, BQU57, and RBC5 (as a negative control) on human lung cancer lines, H2122, H358, H460 and Calu6. Ral promotes anchorage-independence[1,20], therefore we measured cell growth in soft agar. We examined drug uptake, and found that RBC8, BQU57 and RBC5 were readily taken into cells (Extended Data Fig. 5a–c). In addition, we found that all four lines were sensitive to K-Ras siRNA depletion (Extended Data Fig. 6a, b) but only H2122 and H358 were sensitive to Ral knockdown (Extended Data Fig. 6c, d). We used this characteristic to assess the specificity of the compounds for inhibiting Ral. Colony formation in soft agar showed that the Ral-dependent lines H2122 and H358, but not H460 or Calu6, were sensitive to RBC8 and BQU57 treatment (Fig. 3a, b). The IC_{50} for RBC8 is 3.5 μM in H2122 and 3.4 μM in H358; for BQU57 2.0 μM in H2122 and 1.3 μM in H358. The inactive control compound RBC5 did not inhibit growth of any of these cell lines (Extended Data Fig. 5d). Additionally, a Ral pull-down assay using RalBP1 agarose beads[8] showed that RBC8 and BQU57 but not RBC5 inhibited both RalA and RalB activation in both the H2122 and H358 cell lines (Extended Data Fig. 5e).

To further examine the specificity of the compounds for Ral, Ral A and B were knocked down in H2122 and H358 cells with siRNA. RBC8 or BQU57 treatment showed no further inhibition of colony formation after Ral knockdown (Fig. 3c–f, Extended Data Fig. 6e). This supports the conclusion that inhibition of cell growth by these compounds depends on Ral proteins. Lastly, overexpression of a constitutively active (GTP-form[22]) $RalA^{G23V}$ or $RalB^{G23V}$, which do not bind these compounds (Extended Data Fig. 3d, 4b), mitigated inhibition of H2122 and H358 cell growth by these compounds (Fig. 3g–j, Extended Data Fig. 6f). Together, these data provide evidence that RBC8 and BQU57 act specifically through the GDP-bound form of Ral proteins.

Inhibition of Ral activity and tumor growth were evaluated in human lung cancer mouse xenograft models. Pharmacokinetics (PK) of RBC8 and BQU57 were analyzed in mice. Serum concentrations were determined using LC-MS/MS methods after intraperitoneal injection. RBC8 and BQU57 showed favorable properties that define good drug candidates (Extended Data Fig. 7a). We then determined compound entry into tumor tissue 3h after dosing. As shown in Extended Data Fig. 7b–c, the compounds were detected in tumor tissue *in vivo*. To test the effect of Ral inhibitors on xenograft tumor growth, nude mice were inoculated subcutaneously with H2122 human lung cancer cells and treated intraperitoneally

with 50 mg/kg/d of RBC8 for 21 days (except weekends). RBC8 inhibited tumor growth (Fig. 4a, Extended Data Fig. 7d) to a similar extent as dual knockdown of RalA and RalB (Fig. 4b). A second lung cancer line, H358 yielded similar results (Extended Data Fig. 7e). BQU57 was tested *in vivo* at several different doses 10, 20, and 50 mg/kg/d and dose-dependent growth inhibition effects were observed (Fig. 4c).

Lastly, to further evaluate specificity for Ral GTPases, H2122 xenograft tumors (median size 250 mm^3) were collected 3h after a single intraperitoneal injection of RBC5 (50 mg/kg), RBC8 (50 mg/kg) or BQU57 (10/20/50 mg/kg) and activation of Ral in the extracts was analyzed in RalBP1 pull-down assays. Both RalA and RalB were significantly inhibited by RBC8 (Extended Data Fig. 8a–d) and BQU57 (Fig. 4e) but not by the inactive compound RBC5 (Extended Data Fig. 8e, f). By contrast, no inhibition of Ras and RhoA activity was observed (Fig. 4e).

One reason for the failures to date to obtain clinically useful inhibitors for Ras and other related GTPases is the highly conserved guanine nucleotide binding site that has high affinity for the guanine nucleotides GDP/GTP present at millimolar concentrations in cells, and would out-compete ligands for this site. Similar considerations delayed development of protein kinase inhibitors, and indeed some of the best kinase inhibitors proved to not be competitive with ATP, but are allosteric inhibitors that lock the conformation of kinases such as MEK in a closed state[23]. Recently, three studies used similar fragment-based small molecule screening to identify compounds that bind sites on the K-Ras surface and block its SOS-mediated activation[24–26] suggesting the approach has some promise.

Although our initial library screening was based on RalA structure, the selected compounds also bound RalB, which is not surprising given the similarity of the amino acid sequences and predicted structures. Molecular docking could not be performed on RalB-GDP since only the RalB-GNP structure is available. However, NMR experiments with RalB-GDP demonstrated interactions within the allosteric site. Moreover, the selected compounds inhibited the activity of both RalA and RalB in cell culture and in human tumor xenografts. Although distinct roles of RalA and RalB in tumorigenesis and metastasis has been proposed [1,8,12,13], genetically engineered mouse models revealed substantial redundancy for Ral proteins in tumorigenesis[12]. These results support the clinical utility of compounds that inhibit both GTPases. Though additional medicinal chemistry optimization is required, these Ral inhibitors represent a first generation of valuable tools for elucidating Ral signaling and developing novel agents for cancer therapy.

METHODS

Materials

Human bladder cancer cell line J82 and lung cancer cell lines H2122, H358, H460, and Calu6 were obtained from ATCC. All cell line were fingerprinted by STR profiling and tested for mycoplasma contamination. Antibodies: RalA (BD Biosciences, #610222), RalB (Millipore #04–037), and FLAG tag (Novagen #71097). siRNA against human RalA and RalB or both were obtained from Dharmacon (Boulder, CO) using published sequences[8]. Activity assay kits for Ras (#BK008) and RhoA (#BK036) were obtained from Cytoskeleton

(Denver, CO). All RBC compounds were purchased from ChemDiv (San Diego, CA). Unless otherwise notified, all chemicals were obtained from Sigma-Aldrich Chemical Company.

Computational-based molecular modeling

The crystallographic coordinates of the 2.66Å human RalA-GDP (PDB: 2BOV)[27], RalA-GNP in complex with exo84 (PDB: 1ZC4)[28], RalA-GNP in complex with sec5 (PDB: 1UAD)[29] crystal structures were obtained from the RCSB Protein Data Bank (http://wwww.rcsb.org). AutoDock4 was used for the initial library screening. The ChemDiv library [v2006.5, 500,000 compounds excluding those possessing reactive groups, known ADME/toxicity, physicochemical properties lie outside 'drug-likeness' parameters (Lipinski's rule of 5 and Veber's Rule of 2) at pH 7] was downloaded from ZINC database[19] and docked into the identified site on RalA-GDP using rigid docking protocols. Ligand molecules were assigned Gasteiger charges and polar hydrogen atoms by the ligand preparation module provided in the AutoDockTools. The Lamarckian genetic algorithm in AutoDock4 was used to evaluate ligand binding energies over the conformational search space. We then ranked compounds based on binding energy and selected top hits for evaluation.

RalA ELISA

J82 cells stably overexpressing FLAG-RalA were plated 800,000 cells per well in 6-well plates and allowed to incubate for 16 h. Cells were treated with 500 μl of fresh medium containing test compounds (50 μM) or DMSO control (1.0 h; 37°C). Cells were then washed with ice-cold PBS and collected into ice-cold lysis buffer (750 μl containing 50 mM Tris, pH 7.5, 200 mM NaCl, 1% Igepal ca-630, 10 mM MgCl2, and protease inhibitors). The lysate was cleared by centrifugation and the supernatants were then flash-frozen and stored at −80°C until testing. For the ELISA assay, HisGrab nickel coated 96-well plate strips (Pierce, #15142) were washed three times with ELISA buffer (200 μl consisting of 50 mM Tris, pH 8.0, 150 mM NaCl, 0.5% Tween 20, and 10 mM $MgCl_2$). RalBP1 (0.5 μg/100 μl) was then added to the wells and incubated with rocking (2.0 h RT). The plates were then washed three times with 200 μl ELISA buffer. The plates were placed on ice and lysates, or lysis buffer control (100 μl), were added to the wells in quadruplicate. The plates were then incubated overnight with rocking at 4°C followed by two washes with ice-cold ELISA buffer. Mouse anti-FLAG (Sigma, F1804) antibody (1:20,000 in ELISA buffer) was then added at 100 μl per well and incubated (1.0 h, 4°C). After three washes, goat anti-mouse antibody conjugated to HRP (Pierce, #31430) (1:2,500) was added at 100 μl per well and incubated (1.0 h, 4°C). HRP substrate (Vector Laboratories, #SK-4400) was added to each well at 100 μl after three washes and incubated for 1.0 h at RT. The reactions were stopped by adding sulfuric acid (100 μl, 2N). Absorbance was read at OD450 on a Biotek Synergy H1 plate reader (BioTek Instruments, Inc., Winooski, VT); Absorbance was corrected for background absorbance by subtracting the reading for the same well at OD540.

Mouse Embryonic Fibroblasts Spreading Assay

The MEF spreading assay was performed according to published procedures[20]. Briefly, wild type or caevolin$^{-/-}$ mouse embryonic fibroblasts were starved for 24 h, detached from

culture plates with Accutase (Innovative Cell Technologies Inc., San Diego, CA), resuspended in DMEM with 0.2% serum and 0.5% methyl cellulose, and held in suspension (90 min, 37°C). While in suspension, cells were treated with inhibitor or DMSO for 1.0 h. After treatment, cells were rinsed once with DMEM containing 0.2% serum and equal numbers of cells from all treatments were added to 24-well plates that had been coated overnight (4°C, 2.0 μg/mL human fibronectin). Cells were allowed to spread for 30 min and then fixed with formaldehyde using standard protocols. To enable visualization, cells were labeled with Lava Cell (Active Motif) and visualized on a Nikon TE300 fluorescence microscope. Three distinct regions of each well were imaged and cell spread area quantitated using ImageJ.

NMR spectroscopy

RalB (Q72L mutant) in a pET16b (Novagen) plasmid was a kind gift from Dr. Darerca Owen (Cambridge University). RalB was purified as previously described[21], with additional steps for loading with GDP or the non-hydrolyzable form of GTP, GMPNPP (GNP, Sigma-Aldrich) which was done as previously described[30]. Uniform $^{13}C^{15}N$-double labeled protein was produced in M9 media supplemented with ^{15}N-NH_4Cl and ^{13}C-glucose. Samples were prepared for NMR in 50 mM sodium phosphate, pH 7.6, 100 mM NaCl and 1.0 mM $MgCl_2$. All NMR experiments were recorded on an Agilent 900 MHz system at 25 °C. Resonance assignments for the RalB-GNP complex were obtained from previously published studies deposited in Biological Magnetic Resonance Bank (BMRB, code: 15230). Chemical shift assignments of the RalB-GDP complex were obtained independently using HNCACB, CBCA(CO)NH and COCNH-TOCSY experiments. All NMR data was processed using NMRPipe[31] and analyzed using CCPNMR analysis program[32]. Assignment were obtained by automated assignment using PINE[33] followed by manual verification. ^{15}N-HSQC experiments were used to monitor amide shifts from the RalB protein (100 μM) following the addition of compound reconstituted in deuterated DMSO. DMSO concentrations in the final sample were 0.5% or 1%; control samples were made with 0.5% or 1% deuterated DMSO and all samples containing compounds were compared to their corresponding DMSO control. Normalized chemical shift changes were calculated according to the equation $\Delta\delta = \text{sqrt}\ (\Delta\delta H^2 + 0.15*\Delta\delta N^2)$.

Isothermal Titration Calorimetry (ITC) and Surface Plasma Resonance (SPR)

ITC experiments were carried out using the MicroCal iTC200 system. RalB protein was purified as described above. Both protein and drug were prepared in 50 mM sodium phosphate, pH 7.6, 100 mM NaCl, and 1.0 mM $MgCl_2$. Final DMSO concentration was adjusted to 1%. RalB-GDP protein (300 μM) were loaded into the syringe and titrated into drug (25 μM) or buffer alone as control. All experiments were carried out at 25 °C. SPR experiments were carried out using the Biacore 3000 system. RalB protein purified as above. Running buffer contained PBS, pH 7.4, 1.0 μM GDP, 2.0 mM $MgCl_2$, and 3% DMSO. Regeneration buffer contained PBS, pH 7.4, 1.0 μM GDP, and 2.0 mM $MgCl_2$. RalB-GDP protein was immobilized onto CM5 chip; samples of compound BQU57 in running buffer were injected at 30 μL/min for 60 s contact time followed by 5.0 minute regeneration.

Guanine Nucleotide Binding

His-RalA (100 ng) was incubated with gamma-labeled ^{32}P-GTP (8 nM assay concentration) and either DMSO or individual compounds (50 μM assay concentration) dissolved in DMSO in the presence of EDTA (20 mM) for 15 min at 30°C. The reaction was stopped by dilution into excess MgCl2, and the incorporation of radiolabeled nucleotide was measured by filter binding[34]. ^{32}P-GTP (alpha-labeled) was converted to ^{32}P-GDP by nucleotide diphosphokinase, and used for the binding assay with GDP.

In vitro growth of human cancer cells

Growth inhibition on human lung cancer cells by the compounds were measured under anchorage-independent conditions in soft agar. Cells were seeded into 6-well plates (coated with a base layer made of 2.0 ml of 1% low-melting-point agarose) at 15,000 cells per well in 3.0 ml of 0.4% low-melting-point agarose containing various concentration of drug. Two to four weeks (depending on cell line) after incubation, cells were stained with 1.0 mg/ml Nitro Blue Tetrazolium and colonies were counted under a microscope. The IC_{50} values were defined as the concentration of drug that resulted in 50% reduction in colony number compared to DMSO treated control. For growth effects induced by siRNA treatment, cells were transfected with 50 nM siRNA against RalA, RalB or both (RalA/B) using methods and sequences described[8]. After 48 hr, cells were subjected to the soft agar colony formation assay as describe above. For the chemo-genetic experiments, siRNA treated cells were seeded into soft agar in the presence of various concentrations of drug. For the overexpression experiments, H358 cells stably overexpressing FLAG, FLAG-RalA^{G23V} or FLAG-RalB^{G23V} were generated and cells were subjected to the soft agar colony formation assay in the presence of drug. Attempts to stably overexpress FLAG-RalA^{G23V} or FLAG-RalB^{G23V} in H2122 cells were unsuccessful and the rescue experiments with H2122 were carried out 48 hr after transient transfection with FLAG, FLAG-RalA^{G23V} or FLAG-RalB^{G23V} using agar colony formation assay in the presence of drug.

Cellular uptake, Pharmacokinetics and Pharmacodynamics studies

To quantitate how well the compounds get into cells, H2122 human lung cancer cells were seeded at 3×10^5 cells per well in 6-well plates and let sit for 16 h. Compounds (10 μM) were individually dosed in triplicate; cells were then collected into 800 μl ice-cold ACN:MeOH:H_20 (1:1:1) at different time points (1, 5, 15, 30 and 60 min). Drug concentrations in cell lysates were then determined using LC/MS-MS methods described below. The pharmacokinetics of RBC8 and BQU57 were determined in nude mice following a single i.p. dose (50 mg/Kg). Blood samples were collected into EDTA-coated tubes at time intervals from 15 min to 5 h post-dose (9 time points) and centrifuged at 1,500 g for 15 minutes to generate plasma samples. Pharmacokinetic parameters including area under the curve (AUC), C_o, and $t_{½}$ were estimated using non-compartmental methods. The pharmacodynamics of compounds were determined in tumor-bearing nude mice following a single dose of 50 mg/Kg given i.p. Tissue samples were collected 3.0 h after injection of RBC8 or BUQ57. Tissue samples were then homogenized with two weight volumes of phosphate buffer (pH 7.4). HPLC-MS/MS methods to quantify RBC8 and BQU57 in plasma and tissues were developed. Plasma or homogenized tissue samples were extracted with

ACN/MeOH:H_20 (4:1), mixed and centrifuged. The supernatants were transferred into individual wells of a 96-well plate. The 96-well plate was placed into the LEAP auto-sampler (LEAP Technologies; Carrboro, NC) cool-stack (6.0 ± 0.1 °C) and immediately analyzed using a Shimadzu HPLC (Shimadzu Scientific Instruments, Inc.; Columbia, MD) equipped with a Zorbax extended-C18 50 × 4.6 mm, 5 micron column (Agilent Technologies) and guard column. The mobile phase consisted of A: 10 mM ammonium acetate, 0.1% formic acid in water, and B: 50:50 ACN/MeOH. An Applied Biosystems Sciex 4000 (Applied Biosystems; Foster City, CA) was used for compound detection. Standard curves were prepared by spiking compounds into control plasma and tissues (e.g. liver, brain, kidney, lung, heart, and tumor) and these were used to determine drug concentrations.

Tumor growth in mice

All experiments were approved by the University of Colorado Denver Animal Care and Use Committee and were carried out according to approved protocols. Female athymic nude mice (Ncr *nu/nu*; National Cancer Institute, Fredrick, MD) were received at 5 to 6 weeks of age and were allowed to acclimate for 2 weeks in sterile micro isolator cages with constant temperature and humidity. Mice had free access to food and water. Mice were randomized into 6 per group immediately before use (no blinding was done). H2122 cells in log-phase growth were harvested on the day of use. Cells were suspended in un-supplemented RPMI 1640 medium and 0.1 mL (2×10^5 cells) was injected s.c. four sites per mice. For H358 xenografts, cells (5×10^6) were mixed with matrigel (20% final concentration) and 0.1 mL was inoculated s.c. per site. After cell inoculation, mice were monitored daily, weighed twice weekly and caliper measurements begun when tumors visible. Tumor volume was calculated by $(L \times W^2) / 2$, where L is longer measurement of tumor and W is the smaller tumor measurement. Drug treatment started the day after inoculation. Compounds were dissolved in DMSO and injected i.p. daily except weekends at 10/20/50 mg/kg. No obvious toxicities were observed in the control (DMSO) or drug-treated animals as assessed by difference in body weight between control and drug-treated animals taking tumor size into account.

Ral activity in tumor xenografts

Nude mice were inoculated with 5×10^6 cells H2122 cells s.c. When tumor reached an average of 250 mm^3, mice were randomized into 6 per group (no blinding was done) and were given an i.p. dose of RBC8 or BQU57 at various concentrations. Tumors were then collected 3h after injection of RBC8 or BQU57. RalA and RalB activity in tumor samples were then measured using the RalBP1 pull-down assay kit (Millipore #14–415) as we have described[8,15]. Ras and RhoA activity in tumor samples were measured using the respective pull-down assay kits (Cytoskeleton #BK008 and #BK036). All the activity assays used western blotting as the final readout. For quantification of the immunoblot, bands on each blot were first normalized to respective internal control (10 ng of recombinant Ral, Ras, or Ral protein run in the last lane), the numbers were then compared across different blots each of which represented one treatment condition.

General Statistical Methods

Unless otherwise noted, the significance of difference between control and experimental groups was tested using a two-tailed Student's t test or as otherwise indicated in figure legends.

Extended Data

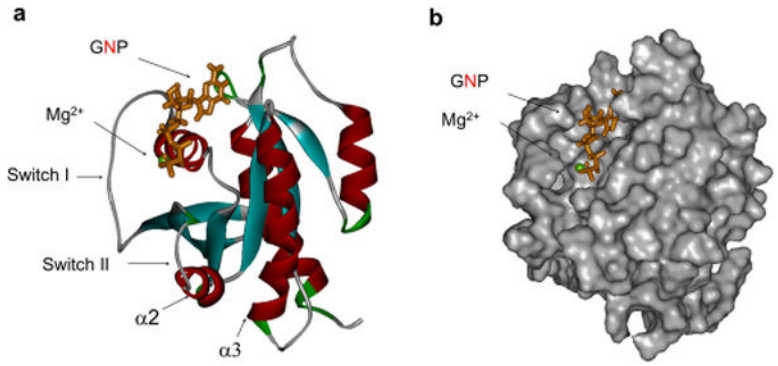

Extended Data Figure 1. Structure model of RalB-GNP

a, Ribbon model showing switch I/II and helix a2/a3. **b**, Surface model showing absence of the allosteric binding site. All models were generated in Accelrys Discovery Studio software using the published RalB-GNP structure (PDB: 2KE5).

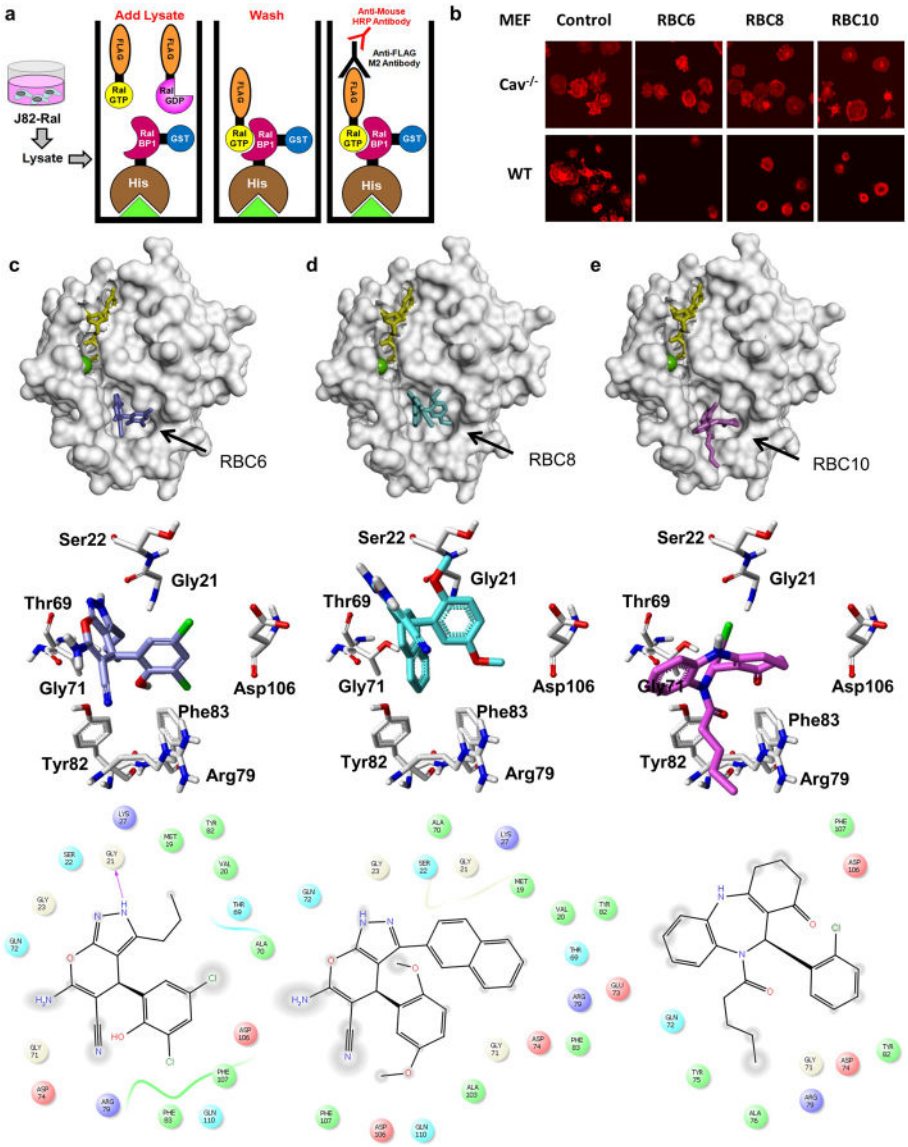

Extended Data Figure 2. Cell-based secondary screening identified RBC6, 8 and 10 as lead compounds for Ral inhibition

a, Scheme of the RalA activity ELISA assay. **b**, Examples of RBC6, RBC8 and RBC10 on the RalA-dependent spreading of MEF cells. Wild-type or caveolin$^{-/-}$ MEF cells were treated with 15 μM of compounds for 1h and subject to the MEF spreading assay as described in Methods. **c–e**, Molecular docking of RBC6 (**c**), RBC8 (**d**), and RBC10 (**e**) into the target site of RalA-GDP. Compounds were shown in stick form and colored purple (RBC6), cyano (RBC8), and pink (RBC10), respectively.

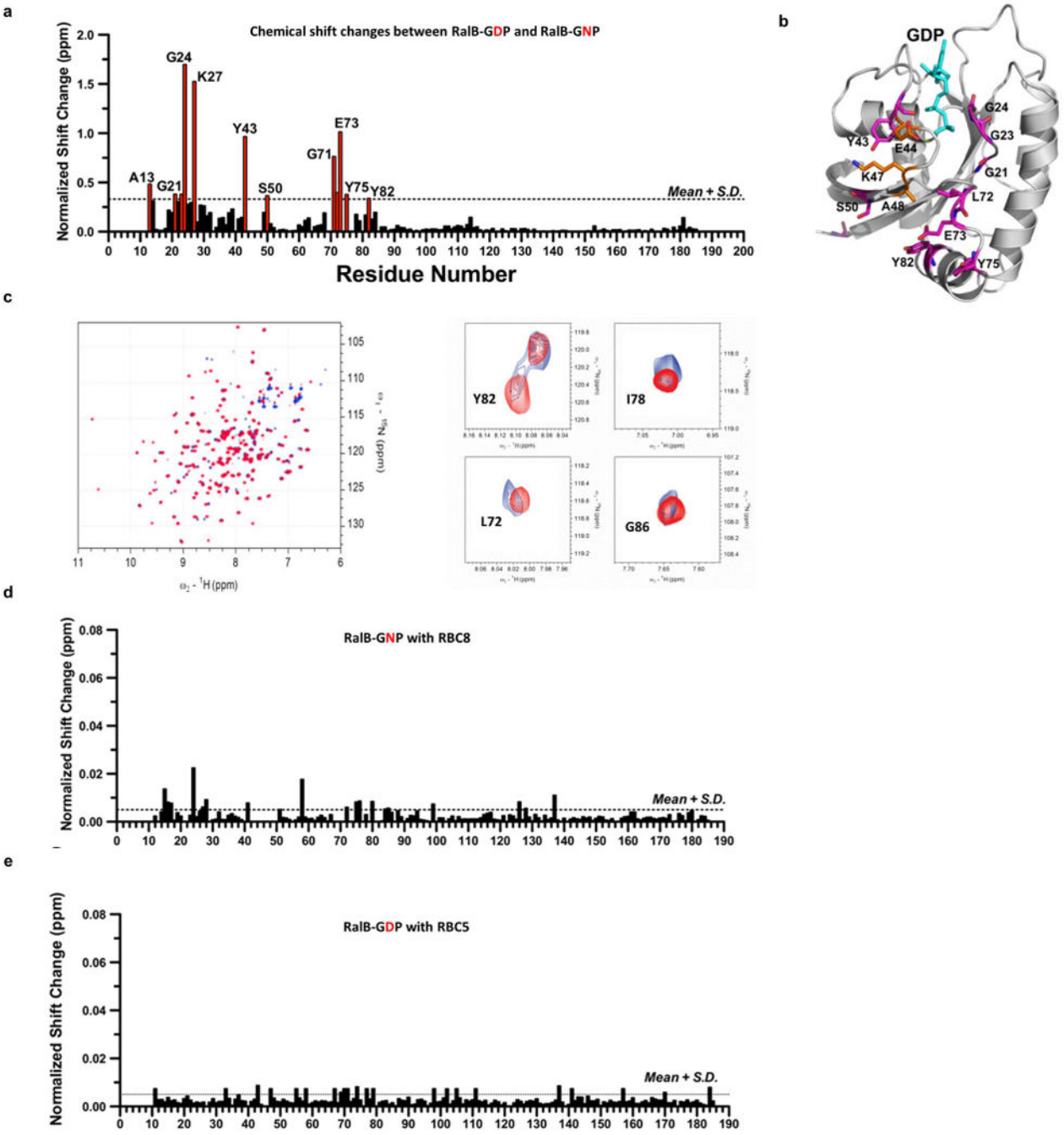

Extended Data Figure 3. Characterization of compound binding to Ral by NMR

a, Plot of chemical shift differences between RalB-GDP and previously published RalB-GNP structure (PDB: 2KE5) as a function of residue number. **b**, Mapping of chemical shift changes onto a homology model of RalB-GDP complex (model based on RalA-GDP PDB ID 1U90). This reveals that changes (magenta) are mostly as a result of changes in the two loops that would otherwise bind to the third phosphate of GTP. GDP is shown as stick model in cyan. **c**, ^{15}N-HSQC spectrum of RalB-GDP (100 μM) in the absence (red) and presence (blue) of 100 μM RBC8. Selected residues exhibiting significant chemical shift

changes are also shown. **d**, Chemical shift changes in RalB-GNP spectrum in presence of 100 μM RBC8. **e**, Chemical shift changes in RalB-GDP (100 μM) spectrum in presence of 100 μM RBC5.

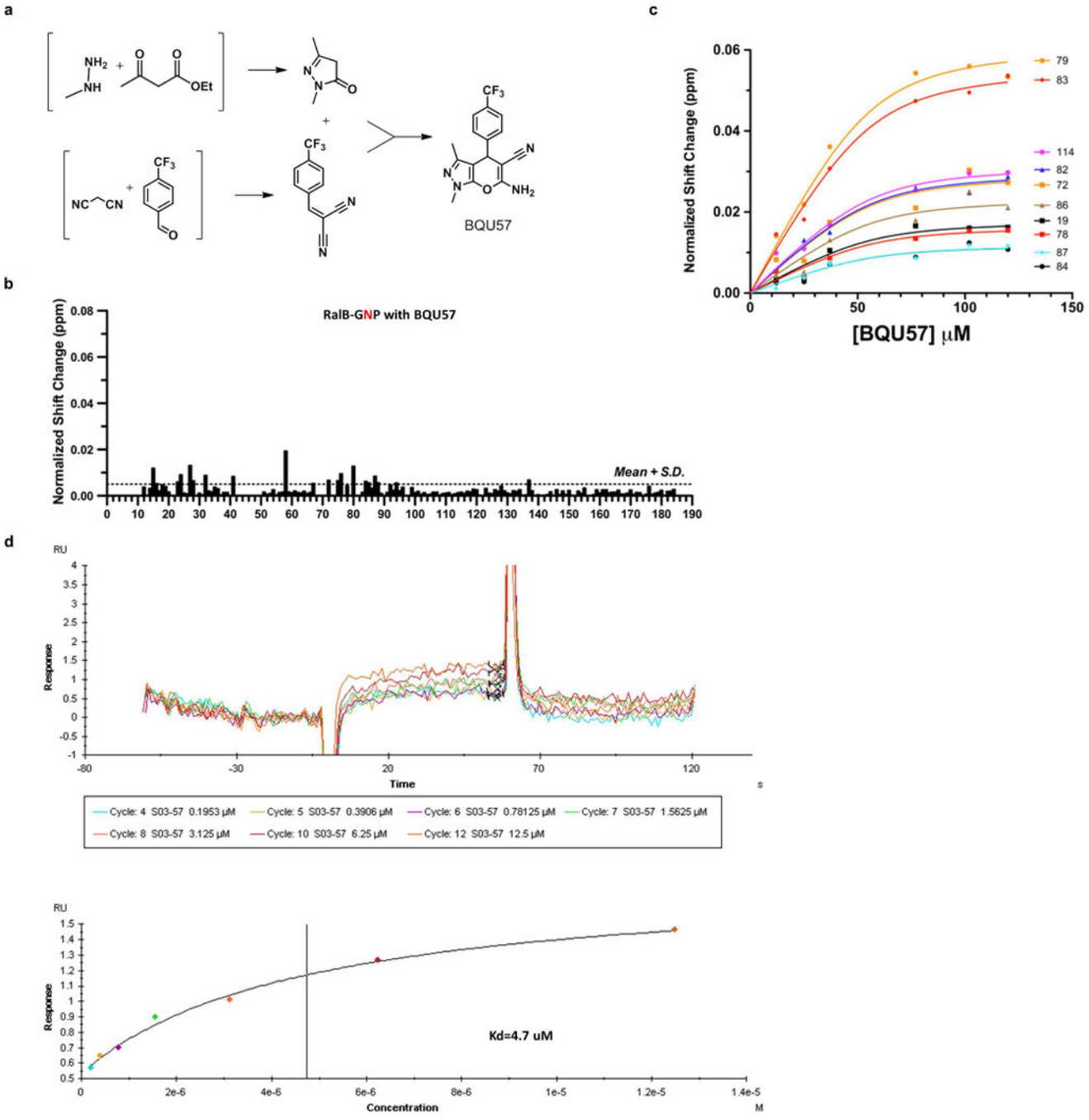

Extended Data Figure 4. Characterization of BQU57 binding to Ral

a, Scheme of the chemical synthesis of BQU57. **b**, Chemical shift changes in RalB-GNP (100 μM) in the presence of 100 μM BQU57. **c**, Plot of 1H-^{15}N-HSQC NMR chemical shift changes of selected residues in RalB-GDP with increasing concentrations of BQU57. **d**,

Determination of K_D for binding between BQU57 and RalB-GDP using surface plasmon resonance. Upper panel: SPR spectrum with increasing concentrations of BQU57; lower panel: fitted binding curve gave a K_D value of 4.7 μM.

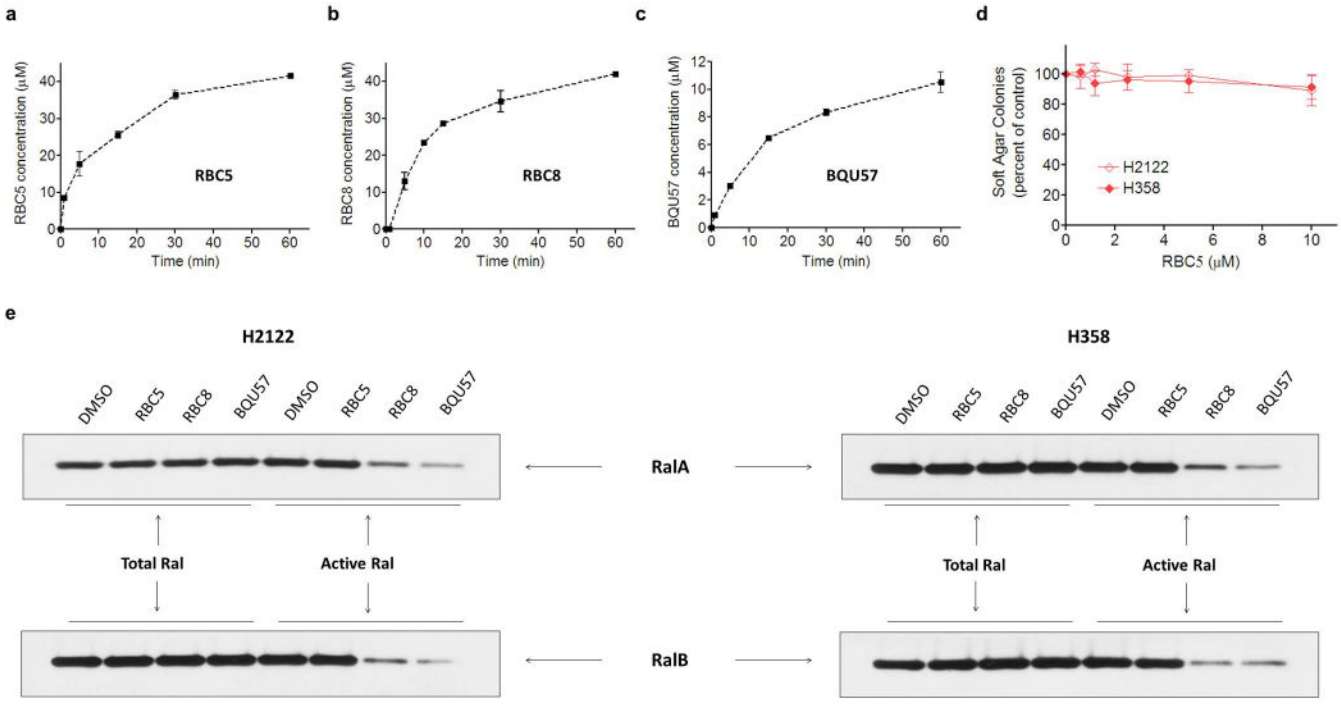

Extended Data Figure 5. Ral inhibitors on human cancer cell lines *in vitro*

a–c, Cellular uptake of Ral inhibitors *in vitro*. H2122 human lung cancer cells were treated with RBC5, RBC8 and BQU57 (10 μM). Cells were collected at various time points (1, 5, 15, 30 and 60 min), and drug concentrations in cells determined using LC/MS-MS methods. Data represents the mean ± SD of triplicate samples. **d**, Effect of RBC5 treatment on the anchorage-independent growth of H2122 and H358 human lung cancer cell lines. Cells were seeded in soft agar containing various concentrations of drug; colonies formed in soft agar were counted after 2–4 weeks. Data represents the mean ± SD of triplicate samples. **e**, Inhibition of Ral activity in H2122 and H358 cells by RBC5, RBC8 and BQU57. Cells were grown under anchorage-independent conditions and treated with 10 μM compounds for 3 hrs. Ral activity in cell lysates were then determined using the pull down assay with RalBP1 agarose beads. Total lysates (20 μg protein) and RalBP1 pull-downs (from 400 μg protein) were analyzed by immune-blotting using antibodies specific for RalA and RalB. Data represent three independent experiments.

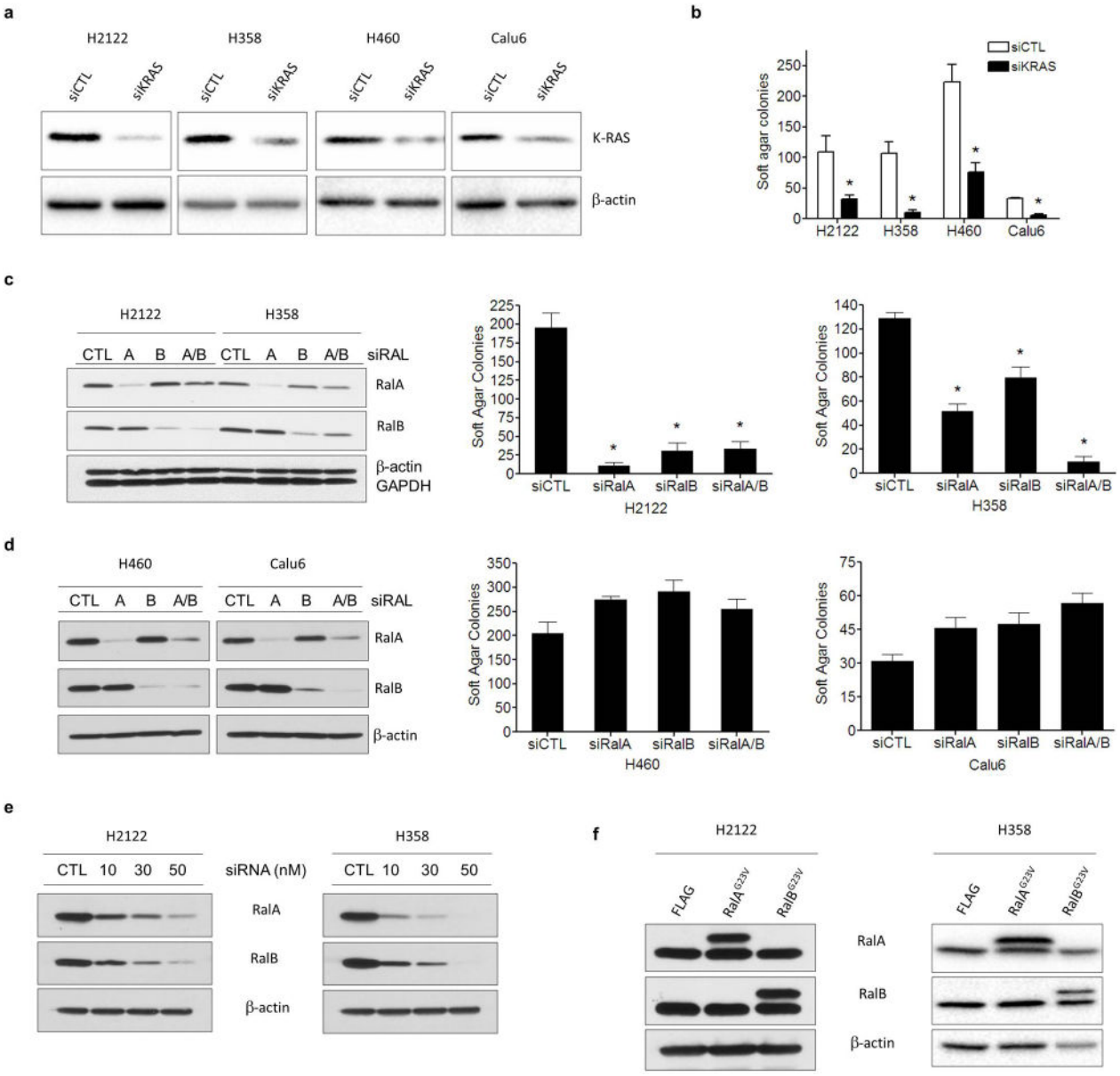

Extended Data Figure 6. Ras and Ral knockdown in human cancer cell lines

a–b, Effect of K-Ras knockdown on anchorage-independent growth of four human lung cancer cell lines. **a**, Immunoblot showing siRNA knockdown of K-Ras in H2122, H358, H460, and Calu6 cell lines 48h after siRNA transfection. **b**, All four lines were sensitive to K-Ras knockdown using the soft agar colony formation assay. Data represents the mean ± SD of triplicate samples. * Statistically different from respective controls as determined by the Student's t-test ($p<0.05$). **c–d**, Effect of Ral knockdown on anchorage-independent growth of four human lung cancer cell lines. Cells were transfected with siRNA against RalA, RalB or RalA/B for 48h and subjected to soft agar colony formation assay. H2122/H358 (**c**) but not H460/Calu6 (**d**) were sensitive to Ral knockdown. Data represents the mean ± SD of triplicate samples. * Statistically different from controls as determined by Dunnett's test ($p<0.05$). **e**, Immunoblots showing knockdown of both RalA and RalB in

H2122 and H358 cell lines 48h after treatment with various concentrations of siRNA. **f**, Immunoblots showing successful overexpression of constitutively active $RalA^{G23V}$ and $RalB^{G23V}$ in H2122 and H358 cells. H2122 cells were transiently transfected with FLAG, FLAG-$RalA^{G23V}$ and FLAG-$RalB^{G23V}$ for 48 h. H358 cells stably overexpressing FLAG, FLAG-$RalA^{G23V}$ and FLAG-$RalB^{G23V}$ were generated by G418 selection.

a

	RBC8	BQU57
Dose (mg/kg) i.p.; n=3	50.0	50.0
Co (μM)	41.2 ± 4.2	41.6 ± 5.1
$T_{1/2}$ (hr)	0.58 ± 0.26	1.50 ± 0.11
$AUC_{0\text{-}5hr}$ (μg • h / mL)	139.6 ± 18.8	28.6 ± 2.1

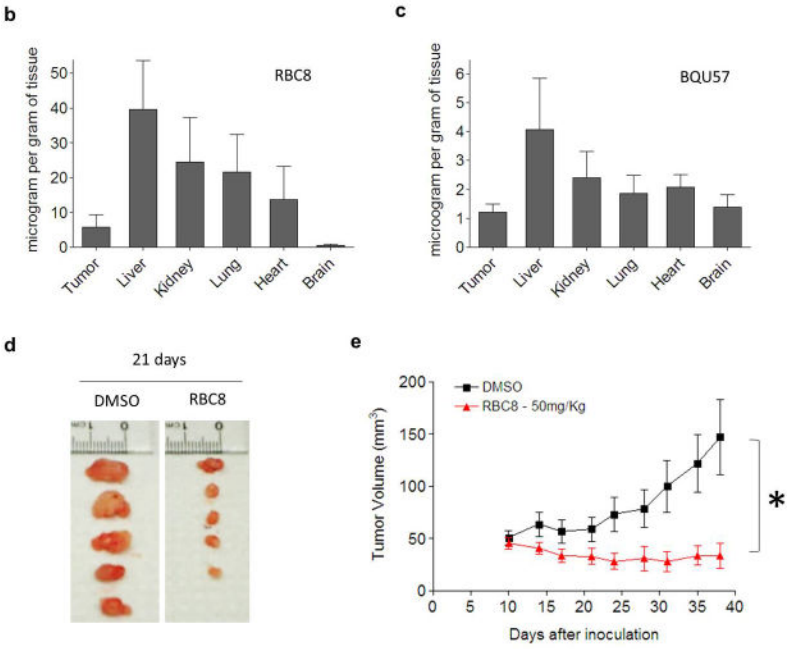

Extended Data Figure 7. Effect of Ral inhibitors on human xenograft models of lung cancer

a, Summary of pharmacokinetic parameters of RBC8 and BQU57 in nu/nu mice. Animal PK parameters were measured based on plasma levels after 50 mg/kg single intraperitoneal dose. Abbreviations used: C_o, extrapolated initial concentration; $T_{1/2}$, half-life; $AUC_{0–5hr}$, area under the curve, zero to five hours. **b–c**, Tissue distribution of RBC8 (**b**), BQU57 (**c**) in nude mice 3h after a single i.p. dose of 50 mg/Kg of drug. Data represent the mean ± SD of 3 mice. **d**, 50 mg/kg/day RBC8 initiated 24h after inoculation inhibited xenograft tumor growth of human lung cancer cell line H2122. Typical tumor appearance at 21 days are shown. **e**, Effect of RBC8 on H358 xenograft models. RBC8 treatment (50 mg/kg/day) initiated 24 h after inoculation inhibited xenograft tumor growth of human lung cancer cell line H358. Data represents the mean ± SEM of 6 mice. Tumor volume in the treatment group was statistically different from controls as determined by the Student's t-test (*$p<0.05$).

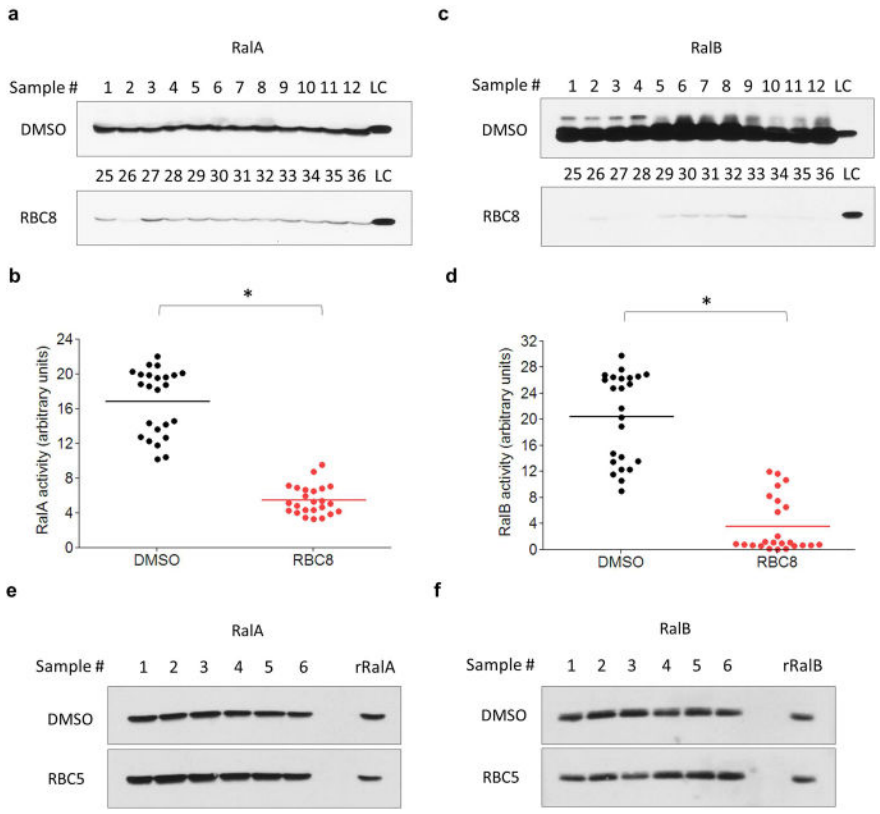

Extended Data Figure 8. Inhibition of Ral activity by RBC8 and RBC5 *in vivo*

a–d, RBC8 inhibited RalA (**a, b**) and RalB (**c, d**) activity in H2122 xenograft tumors. Tumor-bearing nude mice were given a single dose of 50 mg/Kg RBC8 for 3 hrs. The tumors were then collected and Ral activity in tumor lysates measured using the RalBP1 pull-down assay. Immuno-blots from the Ral activity pull-down assay (**a, c**) and quantification (**b, d**) are shown. Each lane represents one tumor sample. Each blot represents one treatment. The last lane in each blot (labeled LC: loading control) was loaded with 10 ng of recombinant human RalA or RalB as internal control for normalization and cross-blot comparison. Band intensity on each blot was first normalized to the internal control and then compared across different blots. Ral activity in the treatment groups were statistically different from controls as determined by student's t-test (*p<0.001, n = 24). **e–f**, RBC5 did not inhibit RalA (**e**) or RalB (**f**) activity in H2122 xenograft tumors. Tumor-bearing nude mice were given a single dose of 50 mg/Kg RBC5 for 3 hrs. The tumors were then collected and Ral activity in tumor lysates measured using the RalBP1 pull-down assay (n=6).

Supplementary Material

Refer to Web version on PubMed Central for supplementary material.

Acknowledgments

This work was supported in part by NIH grants CA091846, CA075115, CA104106, GM47214 and the IUPUI Research Scholar Grant Foundation. The research utilized services of the Medicinal Chemistry Core facility (MFW) housed within the Department of Pharmaceutical Sciences. In part, the MCC has been funded via Colorado Clinical and Translational Sciences Institute grant UL1TR001082 from National Center for Research Resources at

the National Institutes of Health (NCRR/NIH). We acknowledge Dr. Donald S. Backos for assistance with computational modeling Adam Spencer for biochemical assays, Barb Helfrich for assistance with lung cancer cell line culture and the Purdue University NMR core facility.

References

1. Lim KH, et al. Divergent roles for RalA and RalB in malignant growth of human pancreatic carcinoma cells. Curr Biol. 2006; 16:2385–2394. [PubMed: 17174914]
2. Schubbert S, Shannon K, Bollag G. Hyperactive Ras in developmental disorders and cancer. Nat Rev Cancer. 2007; 7:295–308. [PubMed: 17384584]
3. Tsimberidou AM, Chandhasin C, Kurzrock R. Farnesyltransferase inhibitors: where are we now? Expert Opin Investig Drugs. 2010; 19:1569–1580.
4. Roberts PJ, Der CJ. Targeting the Raf-MEK-ERK mitogen-activated protein kinase cascade for the treatment of cancer. Oncogene. 2007; 26:3291–3310. [PubMed: 17496923]
5. Yap TA, et al. Targeting the PI3K-AKT-mTOR pathway: progress, pitfalls, and promises. Curr Opin Pharmacol. 2008; 8:393–412. [PubMed: 18721898]
6. Neel NF, et al. The RalGEF-Ral Effector Signaling Network: The Road Less Traveled for Anti-Ras Drug Discovery. Genes Cancer. 2011; 2:275–287. [PubMed: 21779498]
7. Awasthi S, Sharma R, Singhal SS, Zimniak P, Awasthi YC. RLIP76, a novel transporter catalyzing ATP-dependent efflux of xenobiotics. Drug Metab Dispos. 2002; 30:1300–1310. [PubMed: 12433796]
8. Oxford G, et al. RalA and RalB: antagonistic relatives in cancer cell migration. Cancer research. 2005; 65:7111–7120. [PubMed: 16103060]
9. Lim KH, et al. Activation of RalA is critical for Ras-induced tumorigenesis of human cells. Cancer Cell. 2005; 7:533–545. [PubMed: 15950903]
10. Camonis JH, White MA. Ral GTPases: corrupting the exocyst in cancer cells. Trends in Cell Biology. 2005; 15:327–332. [PubMed: 15953551]
11. Zipfel PA, et al. Ral activation promotes melanomagenesis. Oncogene. 2010; 29:4859–4864. [PubMed: 20562921]
12. Peschard P, et al. Genetic Deletion of RALA and RALB Small GTPases Reveals Redundant Functions in Development and Tumorigenesis. Curr Biol. 2012; 22:2063–2068. [PubMed: 23063435]
13. Martin TD, Der CJ. Differential involvement of RalA and RalB in colorectal cancer. Small GTPases. 2012; 3:126–130. [PubMed: 22790202]
14. Yin J, et al. Activation of the RalGEF/Ral Pathway Promotes Prostate Cancer Metastasis to Bone. Mol Cell Biol. 2007; 27:7538–7550. [PubMed: 17709381]
15. Smith SC, et al. Expression of ral GTPases, their effectors, and activators in human bladder cancer. Clinical Cancer Research. 2007; 13:3803–3813. [PubMed: 17606711]
16. Smith SC, Baras AS, Owens CR, Dancik G, Theodorescu D. Transcriptional signatures of Ral GTPase are associated with aggressive clinicopathologic characteristics in human cancer. Cancer Res. 2012; 72:3480–3491. [PubMed: 22586063]
17. Pautsch A, Vogelsgesang M, Trankle J, Herrmann C, Aktories K. Crystal structure of the C3bot-RalA complex reveals a novel type of action of a bacterial exoenzyme. EMBO J. 2005; 24:3670–3680. [PubMed: 16177825]
18. Shoichet BK. Virtual screening of chemical libraries. Nature. 2004; 432:862–865. [PubMed: 15602552]
19. Irwin JJ, Shoichet BK. ZINC–A free database of commercially available compounds for virtual screening. Journal of Chemical Information and Modeling. 2005; 45:177–182. [PubMed: 15667143]
20. Balasubramanian N, et al. RalA-exocyst complex regulates integrin-dependent membrane raft exocytosis and growth signaling. Curr Biol. 2010; 20:75–79. [PubMed: 20005108]
21. Fenwick RB, et al. Solution structure and dynamics of the small GTPase RalB in its active conformation: significance for effector protein binding. Biochemistry. 2009; 48:2192–2206. [PubMed: 19166349]

22. Hinoi T, et al. Post-translational modifications of Ras and Ral are important for the action of Ral GDP dissociation stimulator. J Biol Chem. 1996; 271:19710–19716. [PubMed: 8702675]
23. Fang Z, Grutter C, Rauh D. Strategies for the selective regulation of kinases with allosteric modulators: exploiting exclusive structural features. ACS Chem Biol. 2013; 8:58–70. [PubMed: 23249378]
24. Sun Q, et al. Discovery of small molecules that bind to K-Ras and inhibit Sos-mediated activation. Angew Chem Int Ed Engl. 2012; 51:6140–6143. [PubMed: 22566140]
25. Maurer T, et al. Small-molecule ligands bind to a distinct pocket in Ras and inhibit SOS-mediated nucleotide exchange activity. Proc Natl Acad Sci U S A. 2012; 109:5299–5304. [PubMed: 22431598]
26. Shima F, et al. In silico discovery of small-molecule Ras inhibitors that display antitumor activity by blocking the Ras-effector interaction. Proc Natl Acad Sci U S A. 2013; 110:8182–8187. [PubMed: 23630290]
27. Holbourn KP, Sutton JM, Evans HR, Shone CC, Acharya KR. Molecular recognition of an ADP-ribosylating Clostridium botulinum C3 exoenzyme by RalA GTPase. Proc Natl Acad Sci U S A. 2005; 102:5357–5362. [PubMed: 15809419]
28. Jin R, et al. Exo84 and Sec5 are competitive regulatory Sec6/8 effectors to the RalA GTPase. EMBO J. 2005; 24:2064–2074. [PubMed: 15920473]
29. Fukai S, Matern HT, Jagath JR, Scheller RH, Brunger AT. Structural basis of the interaction between RalA and Sec5, a subunit of the sec6/8 complex. EMBO J. 2003; 22:3267–3278. [PubMed: 12839989]
30. Thompson G, Owen D, Chalk PA, Lowe PN. Delineation of the Cdc42/Rac-binding domain of p21-activated kinase. Biochemistry. 1998; 37:7885–7891. [PubMed: 9601050]
31. Delaglio F, et al. NMRPipe: a multidimensional spectral processing system based on UNIX pipes. J Biomol NMR. 1995; 6:277–293. [PubMed: 8520220]
32. Vranken WF, et al. The CCPN data model for NMR spectroscopy: development of a software pipeline. Proteins. 2005; 59:687–696. [PubMed: 15815974]
33. Bahrami A, Assadi AH, Markley JL, Eghbalnia HR. Probabilistic interaction network of evidence algorithm and its application to complete labeling of peak lists from protein NMR spectroscopy. PLoS Comput Biol. 2009; 5:e1000307. [PubMed: 19282963]
34. Steggerda SM, Paschal BM. The mammalian Mog1 protein is a guanine nucleotide release factor for Ran. J Biol Chem. 2000; 275:23175–23180. [PubMed: 10811801]

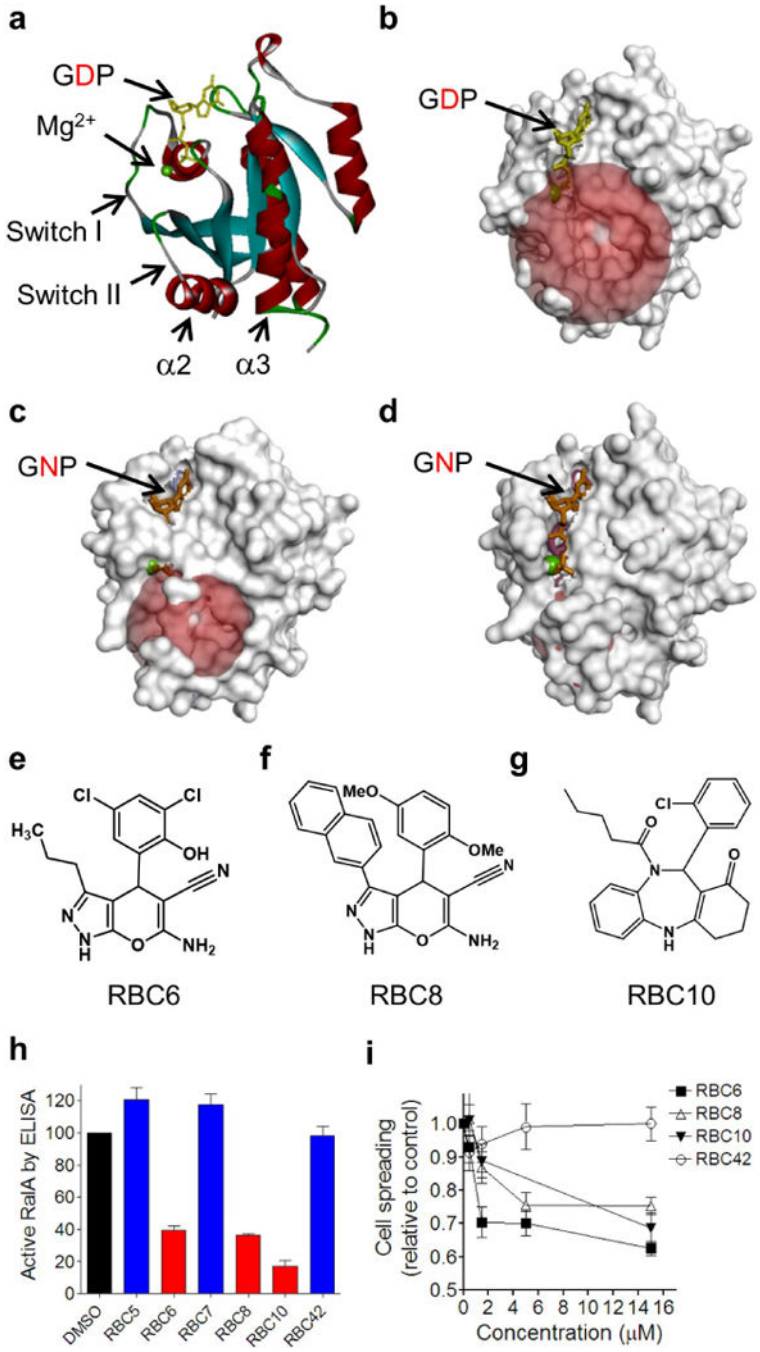

Figure 1. Structure-based in silico library screening and cell-based secondary screening identified RBC6, 8 and 10 as lead compounds for Ral inhibition

a–b, Structural model of RalA-GDP in ribbon (**a**) or surface (**b**) representations**. c–d**, Surface representations of RalA-GNP in complex with exo84 (**c**, exo84 not shown), and RalA-GNP in complex with sec5 (**d**, sec5 not shown). The red sphere/surfaces indicated the water accessible area in the binding cavity. All models were generated in Accelrys Discovery Studio software using published structures. **e–g**, chemical structure of RBC6 (**e**), RBC8 (**f**) and RBC10 (**g**). **h**, RalA ELISA result of top hits and three ineffective compounds

(RBC5, RBC7 and RBC42) identified by computational screening. J82 cells overexpressing FLAG-RalA were treated with compounds for 1h and then subjected to RalA ELISA as described in Methods. Data represent mean ± SD of three replicates. **i**, Dose response effect of RBC6, RBC8 and RBC10 on the RalA-dependent spreading of MEF cells. MEF cells were treated with 0–15 μM of compounds for 1h and subject to the MEF spreading assay as described in Methods. Data represent mean ± SD of three replicates.

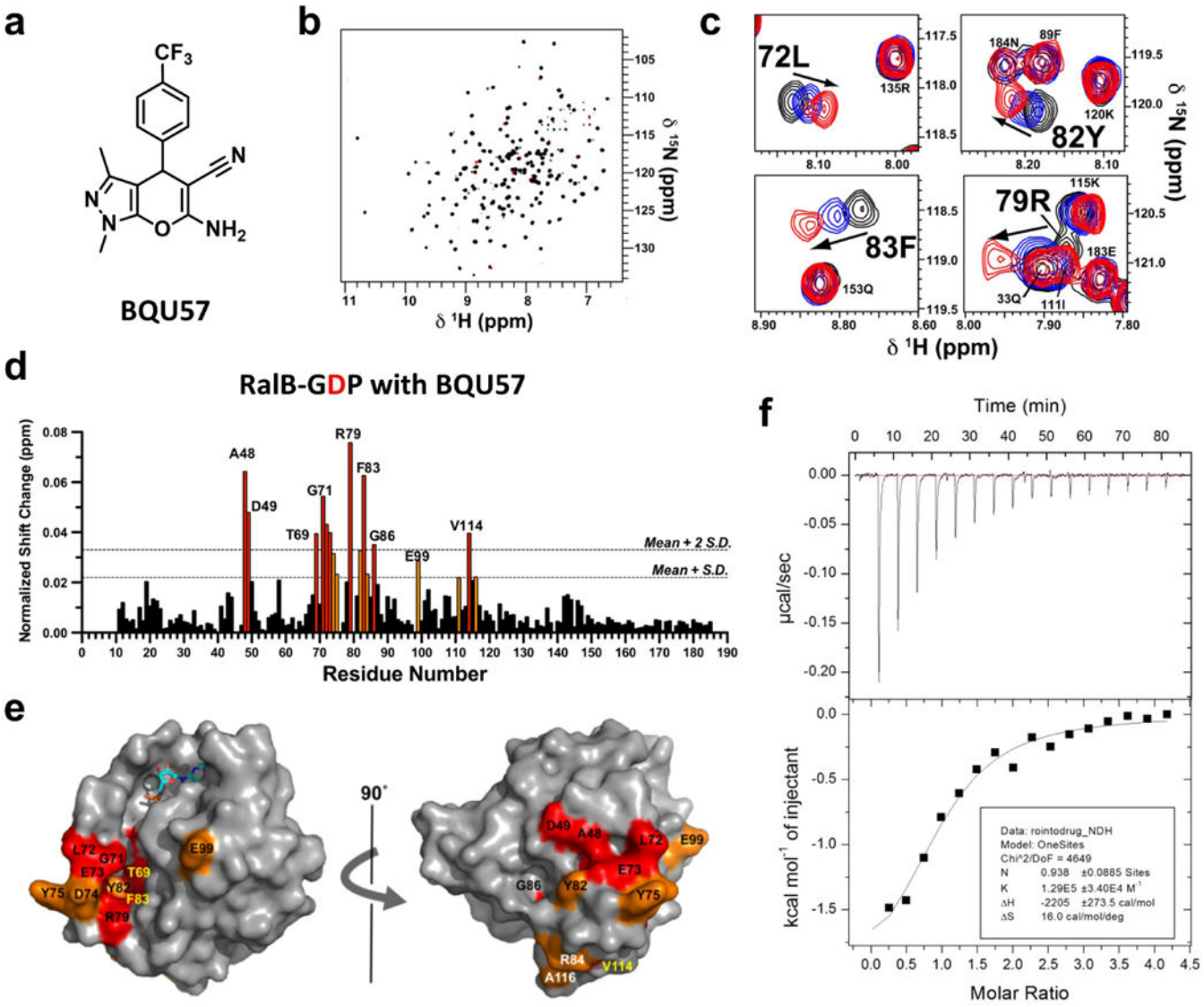

Figure 2. Characterization of compounds binding to Ral

a, Chemical structure of BQU57. **b**, Overlay of the ^{15}N-HSQC spectrum of 100 µM RalB-GDP (black) and in the presence of 100 µM BQU57 (magenta). **c**, Selected residues of RalB-GDP in the absence (black) and presence of increasing concentrations of BQU57 at 40 µM (blue) and 100 µM (red). **d**, Plot of chemical shift changes as a function of residue number comparing RalB-GDP alone and in in the presence of 100 µM BQU57. (red > mean +2 S.D., orange > mean +1 S.D.) **e**, Residues showing significant chemical shift changes (color coding same as in **d**) mapped to their location on a homology model of RalB-GDP complex generated from the published RalA-GDP structure (PDB: 1U90); GDP is shown as stick representation. **f**, Determination of K_D for binding between BQU57 and RalB-GDP using isothermal titration calorimetry. Data represents three independent experiments.

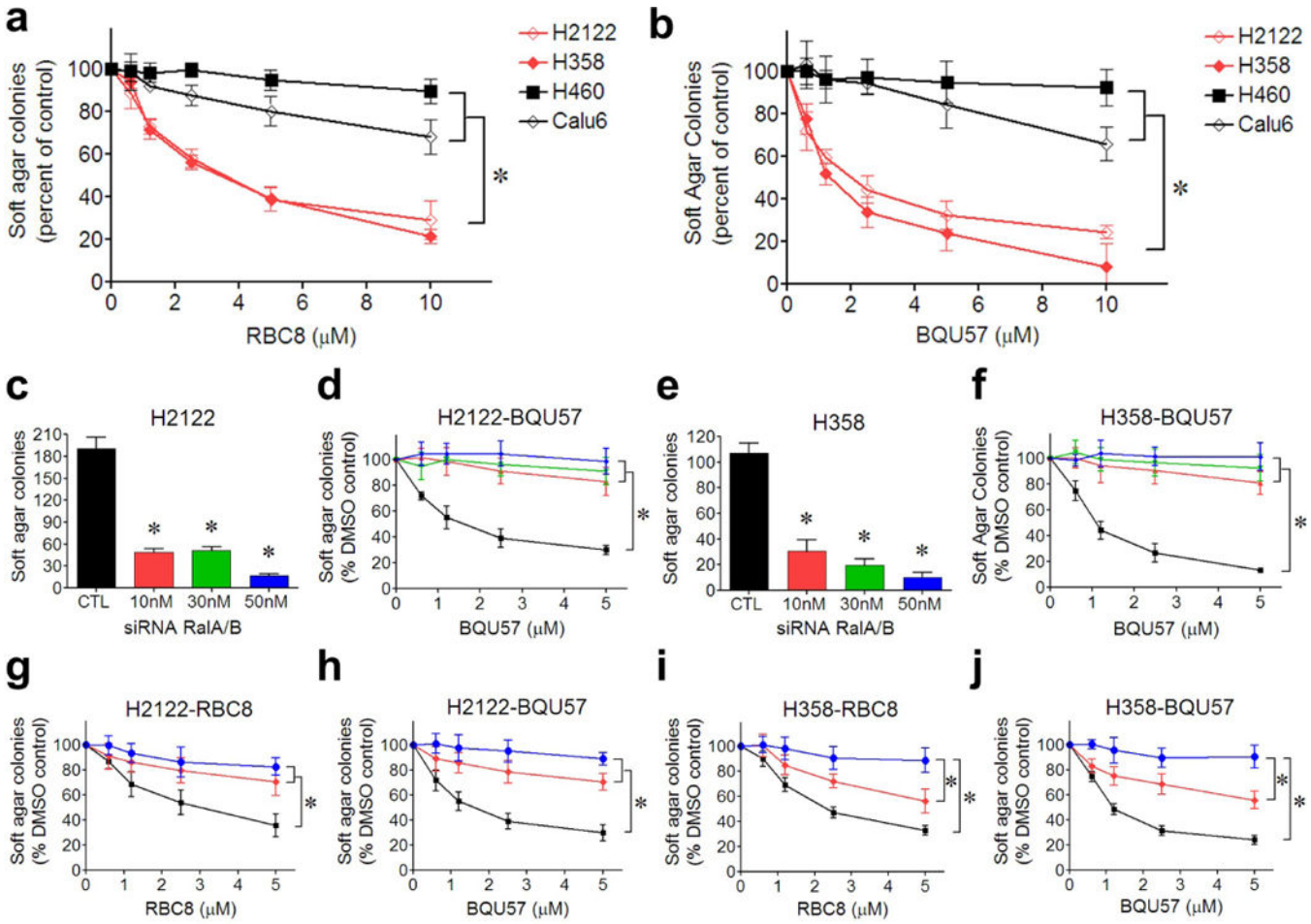

Figure 3. Growth inhibitory activity of Ral inhibitors in human cancer cell lines

a–b, Effect of RBC8 (**a**) and BUQ57 (**b**) treatment on the anchorage-independent growth of 4 human lung cancer cell lines. Cells were seeded in soft agar containing various concentrations of drug; colonies were counted after 2–4 weeks. Cell lines that are sensitive to Ral siRNA knockdown (H2122 and H358) were colored red and cell lines resistant to Ral siRNA knockdown (H460 and Calu6) were colored black. **c–f**, Effect of siRNA knockdown of both RalA and RalB in H2122 (**c, d**) and H358 (**e, f**) cells on drug-induced growth inhibition in soft agar. Cells were transfected with 10/30/50 nM of siRNA for 48h, collected, and subjected to the soft-agar colony formation assay. Effect of siRNA alone on soft agar colony number is shown in **c** (H2122) and **e** (H358); effect of siRNA plus drug treatment on colony formation is shown as percent of DMSO treated control in **d** (H2122) and **f** (H358). Control is colored black, 10 nM red, 30 nM green, and 50 nM blue. **g–j**, Effect of the overexpression of constitutively active $RalA^{G23V}$ and $RalB^{G23V}$ in H2122 (**g, h**) and H358 (**i, j**) cells on drug-induced growth inhibition in soft agar. H2122 cells were transiently transfected with FLAG alone (colored black), FLAG-$RalA^{G23V}$ (colored red) or FLAG-$RalB^{G23V}$ (colored blue) for 48 h before the soft agar colony formation assay. H358 cells were stably transfected with FLAG (black lines), FLAG-$RalA^{G23V}$ (red lines) or FLAG-$RalB^{G23V}$ (blue lines). All results are the mean ± SD of triplicate experiments. * denotes

statistical significant difference between indicated groups ($p<0.05$, student's t-test or Dunnett's test).

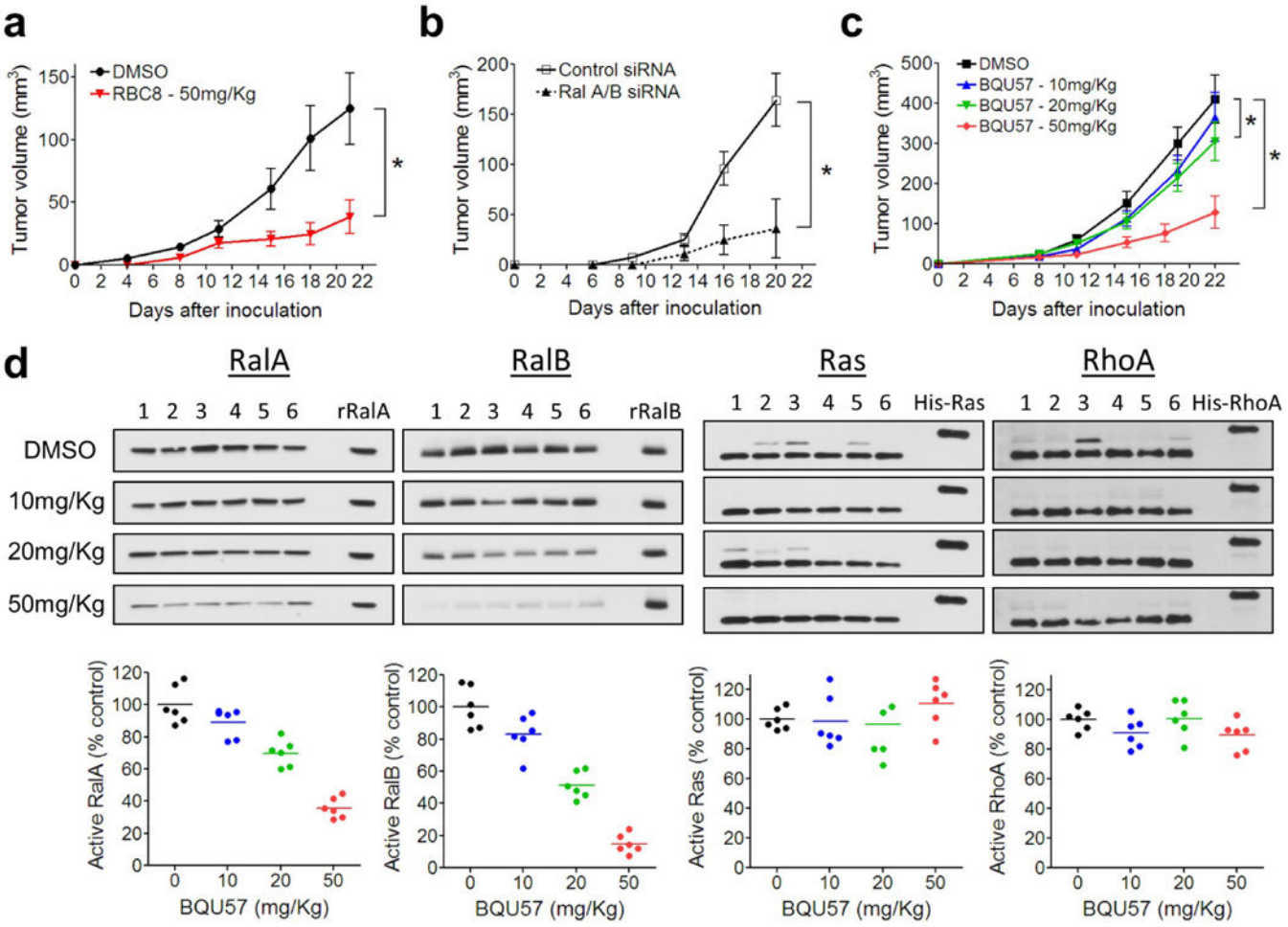

Figure 4. Effect of Ral inhibitors *in vivo*

a, 50 mg/kg/day RBC8 initiated 24h after inoculation inhibited xenograft tumor growth of human lung cancer cell line H2122. **b**, siRNA depletion of both RalA and RalB inhibited the xenograft tumor growth of H2122 cells. Cells were transiently transfected with siRNA for 24h before inoculation into nude mice. **c**, BQU57 treatment (10/20/50 mg/kg/day) initiated 24h after inoculation inhibited xenograft tumor growth of H2122 cells. Data in **a–c** represents the mean ± SEM of 6 mice. *p<0.05 by Student's t-test. **d**, BQU57 treatment inhibited the activity of RalA and RalB but not Ras and RhoA in H2122 xenograft tumor. Tumor-bearing nude mice were given a single dose of 10, 20 or 50 mg/Kg BQU57 for 3h. The activity of RalA, RalB, Ras and RhoA in tumor lysates were then measured using the respective pull-down assay for each GTPase. Immuno-blots from the activity pull-down assays and corresponding quantifications are shown. Each lane represents one tumor sample and each blot represents one treatment group. The last lane in each blot was loaded with 10ng of recombinant human protein as internal control for normalization and cross-blot comparison. Band intensity on each blot was first normalized to the internal control and then compared across different blots. The amount of active Ral/Ras/RhoA are shown as percent of DMSO treated control.